International Journal of Mass Spectrometry 309 (2012) 13–21

Contents lists available at SciVerse ScienceDirect

International Journal of Mass Spectrometry

journal homepage: www.elsevier.com/locate/ijms

Computational fluid dynamics-Monte Carlo method for calculation of the ion trajectories and applications in ion mobility spectrometry

Fenglei Han[a,b], Yongzhai Du[a,b], Shasha Cheng[a,b], Qinghua Zhou[a,b], Chuang Chen[a,b], KeyongHou[a], Weiguo Wang[a], Haiyang Li[a,*]

[a] Dalian Institute of Chemical Physics, Chinese Academy of Sciences, Dalian 116023, People's Republic of China
[b] Graduate School of Chinese Academy of Sciences, Beijing 100039, People's Republic of China

ARTICLE INFO

Article history:
Received 12 July 2011
Received in revised form 18 August 2011
Accepted 18 August 2011
Available online 23 September 2011

Keywords:
Ion trajectory simulation
Modeling
Computational fluid dynamics
SIMION
Ion mobility spectrometry

ABSTRACT

A computational fluid dynamics-Monte Carlo approach (abbreviated as CMC) based on SIMION has been developed for simulating the ions trajectories in both the fluid and electric fields simultaneously, the gas flow effect and collision of the ions with the gas molecules are considered within this approach. Four kinds of physical parameters of the instruments can be obtained by this model: the flow field, the electric field, the ion trajectories and the mobility spectrum. A drift tube ion mobility spectrometer was built and simulated to verify this model. The distribution of gas flow field (velocity, pressure, temperature) was simulated by a 2D geometry. The ions trajectories and ion mobility spectra of the IMS were then calculated. The good agreements between simulation and experiment show that the CMC model has predictive power for modeling ion motion at ambient pressure, and this model can serve as visual aids for intuitively understanding the factors that determine ion transport.

1. Introduction

Many instruments used in analytical chemistry, such as ion mobility spectrometry (IMS) [1,2], differential mobility spectrometry (DMS) [3–6], ion funnel [7,8] and ion trap [9], involve ions moving through gases under the influence of electric field, and are widely used in many fields [10–13]. IMS is a well-known method to analyze chemical substance using gas-phase mobility in a weak electric field [14–16], and is more and more used in the detection of explosives, drugs, chemical warfare agents, biological and medical samples [17–25]. Unlike the mass spectrometry [26,27], which operates in vacuum, IMS detects chemical compounds at atmospheric pressure. The analytes carried by the gas flow are introduced into an ionization chamber, where a radioactive source, discharge source [28], or an UV lamp [29] is used to ionize them. Then the ions are accelerated by an external electrical field with collisions with the neutral gas particles. Because of the difference of mass and collision cross section, the ions arrive at the detector in different time. Although IMS has been developed for over 30 years, but the theory of ion motion in electric field under the influence of gas flow field was less advanced. The common used method in designing and optimizing instruments is a trial-and-error approach, which costs lots of time and money [1]. So a computer simulation model is needed to provide insight of ion transport properties and gas flow field inside the IMS, to optimize the physical parameters of IMS or DMS, such as the geometric shapes of electrodes, electric potentials, frequencies, gas flow rates and pressures, etc. [30–32].

With the development of computer technology and simulation technique, many simulation models have been developed to describe the ion motion in electric field [33–36] or gas flow field [37,38], separately. Some simulation packages also have been developed, such as ITSIM [9,39–41], GEMIOS [42,43], microDMX [44] and SIMION [45] for the ion trajectory simulation. SIMION is a widely used windows-based ion optics simulation program, it can model ion optics and trajectories with two-dimensional (2D) and three-dimensional (3D) electrostatic and magnetic potential arrays in vacuum. However, it is low-performance to simulate the ion motion at atmospheric pressure. Recently, some user defined codes were developed to consider ion collisions [46,47] and viscous damping effect (Stokes law) to describe the ion transport at viscous environment. However, the general viscous flow model did not account for diffusional effects [48], and the ion indeed drifted down the concentration gradient. Dahl has introduced a statistical diffusion simulation (SDS) model to simulate ion trajectories in viscous environment [49,50], its capabilities of simulation ion motion at ambient pressure were demonstrated for IMS by Almirall [51] and for DMS by Smith [52]. Although the gas flow effect included, the SDS model made some special assumptions and approximations, for example, the average ion velocity varied

* Corresponding author. Tel.: +86 411 8437 9509; fax: +86 411 8437 9517.
E-mail address: hli@dicp.ac.cn (H. Li).

1387-3806/$ – see front matter © 2011 Elsevier B.V. All rights reserved.
doi:10.1016/j.ijms.2011.08.017

linearly with the electric field. Some simulation model had to approximate the flow field roughly by a quadratic function [53]. There is no doubt that more accurate method is highly needed to consider the gas flow field effects like velocity, temperature and pressure, etc.

A CFD-Monte Carlo (CMC) simulation model combined the SIMION 8.0 package has been developed and implemented to predict the ions trajectories at ambient pressure under the influence of electric field. This model considers both the gas flow effect and collision of the ions with the gas molecules. With this model, the gas flow distribution and ion trajectories can been seen clearly in an arbitrary geometry device working under the atmospheric pressure. This model was then verified by simulation and experimental results of a home-made IMS. The model has been demonstrated to be sufficiently accurate to provide gas flow, temperature, pressure distribution and ion trajectory information in the analytical instruments.

2. CFD-Monte Carlo modeling approaches

The flowchart of the CFD-Monte Carlo (CMC) model is shown in Fig. 1. The whole process can be described as: a computational geometry is first built based on the physical parameters of the instrument. The so called boundary conditions were defined to common working values, then the gas flow filed, includes velocity field as well as temperature and pressure filed, are obtained from the CFD calculation. The data was then exported and saved in a 'dat' file. A data processing method was developed to re-arrange and process the data file which can be used in the next steps. The electrode geometry was then built to calculate the electric field distribution based on a Laplace solution. After that, the CFD-Monte Carlo model optionally reads in gas velocity, pressure and temperature data for element center locations where collisions happen. When a collision occurs, the particle masses and scattering cross sections are calculated by the model code. The hard-sphere models [54,55] were used to determine the post-collisional ion velocity. The columbic repulsion effect was also considered in this model with a factor repulsion method. At last, the ion trajectories integrations are calculated by solving Newton's equation with higher order Runge–Kutta numerical integration methods. After each simulation, the time of drift that the ions reached the collector was recorded and exported into a 'txt' file. Post-processing software was developed and the spectra can be plotted according to the recorded file after each fly process of grouped ions.

The whole simulation process of the simulation executed using SIMION 8.0 through a 'lua' file defined by the author. All calculations were performed on a desktop computer equipped with Intel Core Q9400 2.67 GHz CPU, 8.0 GB RAM using Windows 7 Enterprise 64 bit operating system.

2.1. Flow and electric field distribution calculation

In our model, the flow field parameters: velocity, pressure and temperature, are calculated by the computational fluid dynamics (CFD) method. The governing equations for fluid dynamics, for viscous flow which are also called Navier–Stokes equations, can be given as follows:

Continuity equation:

$$\frac{\partial \rho}{\partial t} + \nabla \cdot (\rho \vec{V}) = 0. \tag{1}$$

Momentum equations:

$$\frac{\partial (\rho \vec{V})}{\partial t} + \nabla \cdot (\rho \vec{V} \vec{V}) = -\nabla p + \rho \vec{F} + \nabla \cdot \vec{\vec{\sigma}}. \tag{2}$$

Energy equation:

$$\frac{\partial}{\partial t}\left[\rho\left(e + \frac{V^2}{2}\right)\right] + \nabla \cdot \left[\left(e + \frac{V^2}{2}\right)\rho \vec{V}\right] = -\Delta p + \rho \vec{F} \cdot \vec{V} + \nabla \cdot (\vec{V} \cdot \vec{\vec{\sigma}}) + \rho \dot{q} + \nabla \cdot (\lambda \nabla T), \tag{3}$$

where ρ is density, $\vec{V}$ is the velocity vector, p is the static pressure, $\vec{\vec{\sigma}}$ is the stress tensor, e is the internal energy, $\vec{F}$ is the external body force, and λ is the second viscosity coefficient. Stokes made the hypothesis that $\lambda = -2/3\mu$, where μ is the molecular viscosity coefficient.

Standard $k - \varepsilon$ model, introduced firstly by Launder and Spalding [56], is used to calculate the turbulent flow. It is a semi-empirical model based on model transport equations for the turbulence kinetic energy (k) and its dissipation rate (ε). The model transport equation for k is derived from the exact equation, while the model transport equation for ε was obtained using physical reasoning and bears little resemblance to its mathematically exact counterpart. The turbulence kinetic energy k and its rate of dissipation ε are obtained from the following transport equations [57]:

$$\frac{\partial}{\partial t}(\rho k) + \frac{\partial}{\partial x_i}(\rho k u_i) = \frac{\partial}{\partial x_j}\left[\left(\mu + \frac{\mu_t}{\sigma_k}\right)\frac{\partial k}{\partial x_j}\right] + G_k + G_b - \rho\varepsilon - Y_M + S_k, \tag{4}$$

$$\frac{\partial}{\partial t}(\rho \varepsilon) + \frac{\partial}{\partial x_i}(\rho \varepsilon u_i) = \frac{\partial}{\partial x_j}\left[\left(\mu + \frac{\mu_t}{\sigma_\varepsilon}\right)\frac{\partial \varepsilon}{\partial x_j}\right] + C_{1\varepsilon}\frac{\varepsilon}{k}(G_k + C_{3\varepsilon}G_b) - C_{2\varepsilon}\rho\frac{\varepsilon^2}{k} + S_\varepsilon, \tag{5}$$

where G_k represents the generation of turbulence kinetic energy due to the mean velocity gradients, G_b is the generation of turbulence kinetic energy due to buoyancy, Y_M represents the contribution of the fluctuating dilatation incompressible turbulence to the overall dissipation rate, $C_{1\varepsilon}$, $C_{2\varepsilon}$ and $C_{3\varepsilon}$ are constants. σ_k and σ_ε are the turbulent Prandtl numbers for k and ε, respectively. S_k and S_ε are user-defined source terms.

The govern equations above are discretized on structured quadrangular meshes. And the discretization equations are resolved by a SIMPLE algorithm [58], which stands for Semi-Implicit Method for Pressure-Linked Equations. The CFD software FLUENT [57] was used to perform the numerical calculation of the discretization equations. The governing partial differential equations are solved using the finite volume method: a control-volume-based technique is used to convert these equations into a set of algebraic equations that can be solved numerically. This control volume technique integrates the governing equations over each control volume, yielding discrete equations that conserve each quantity on a control-volume basis. Typically, a few thousand of iterations are needed for the program to converge.

The electric field can be determined by solving the Poisson equation by finite difference methods, which can be given as:

$$\nabla^2 V = \nabla \cdot \nabla V = -\frac{\rho_e}{\varepsilon_0}, \tag{6}$$

where ε_0 is the dielectric permittivity and ρ_e is the ionic space charge.

And the electric field intensity can be described as:

$$\vec{E} = -\Delta V. \tag{7}$$

The electrostatic and magnetic field modeling program SIMION mentioned above was used to calculate the potential distribution. In the SIMION software, a finite difference technique called over relaxation method was used to solve the Poisson equation [59].

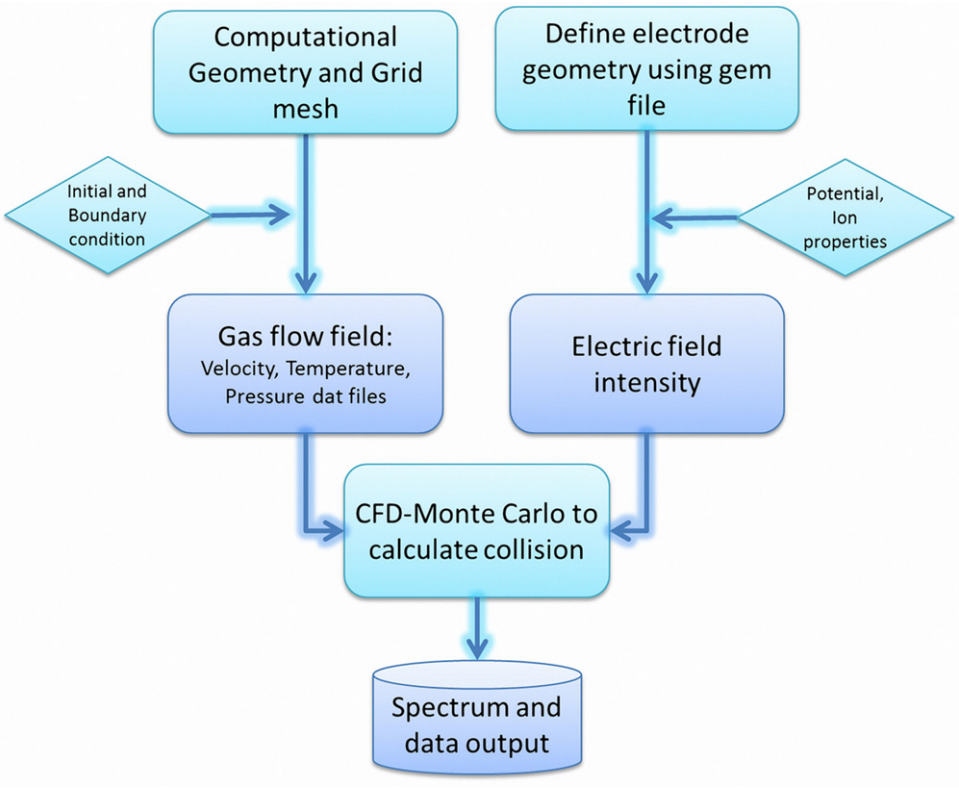

Fig. 1. Flowchart of simulation steps using the CFD-Monte Carlo model.

The columbic repulsion is considered in this model. And factor repulsion method is used to estimate the space charge effect, where each ion represents several ions of the same mass/charge ratio and the total influences applied to the other ions.

2.2. Ion trajectories calculation

CFD-Monte Carlo method was used to model collisions between the ions and molecules with considering the gas flow effect. The detailed algorithm of Monte Carlo can be found in the Ref. [46,47]. As mentioned above, the CFD solution of the Navier–Stokes equation provided the gas velocity, pressure and temperature distribution. And the Laplace/Poisson solution provides the electric field distribution. The flow and electric field data was then used in the calculation of the collision frequency. A local collision probability is computed at each time step based on current ion velocity, ion-gas scattering cross section, local gas flow speed, pressure, and temperature. And these parameters were considered in the model through Eqs. (8)–(10).

According to the Maxwell–Boltzmann kinetic gas theory [55], mean gas speed was calculated velocity using the local temperature T_{local} which was generated by the CFD calculation:

$$\vec{v}_{gas\_mean} = \sqrt{\frac{8kT_{local}}{\pi m_g}}, \tag{8}$$

where m_g is the buffer gas particle mass and k is Boltzmann constant.

The local velocity of the gas flow field $\vec{v}_{local}$ generated from the CFD simulation of the last step was used to adjust the velocity of the gas molecule.

$$\vec{v}_{gas\_ion} = \vec{v}_{gas\_mean} + \vec{v}_{local}. \tag{9}$$

The mean free path is given by:

$$\lambda_{eff} = \frac{1000K \cdot T \cdot v_{ion}}{v_{rel} \cdot \Omega_{eff} \cdot p_{local}}, \tag{10}$$

where p_{local} is the local pressure, which was also calculated in the last CFD simulation; v_{rel} is the mean relative speed between ion and moving background gas molecule; Ω_{eff} is the effective collision cross-section, which can be determined by summation of the spherical-shape cross section and the cross-section contributed from ion-induced polarization of a gas molecule [60].

And the collisions probability between the ions and molecules was calculated by the Monte Carlo method. After each collision, the new ion velocity was converted back into the lab frame. This velocity determined from a collision was used as the ion velocity for the next time step. The whole collision process can be seen in Fig. 2.

2.3. Experimental

A drift tube ion mobility spectrometer was constructed for the verification of the simulation model. The experiment setup, including the attached IMS and the sample introduction system, is schematically illustrated in Fig. 3.

The ion mobility spectrometer used in the experiment was similar to the conventional structure described in our previous paper [28,61], and it mainly included a Ni^{63} ionization source, a Bradbury–Nielson (B–N) gate, a drift tube, a Faraday cup, and a preamplifier. It was made of 11 stainless steel rings separated by Teflon rings. The reaction region was 20 mm long with an i.d. of 14 mm, and the drift region was 55 mm long with an i.d. of 30 mm. The entire drift tube was temperature-controlled up to 100 °C with a tape-heater. A bidirectional flow scheme was used for the IMS, and the sample was diluted and injected into the IMS by a headspace sampling method. Ions of the sample formed in the

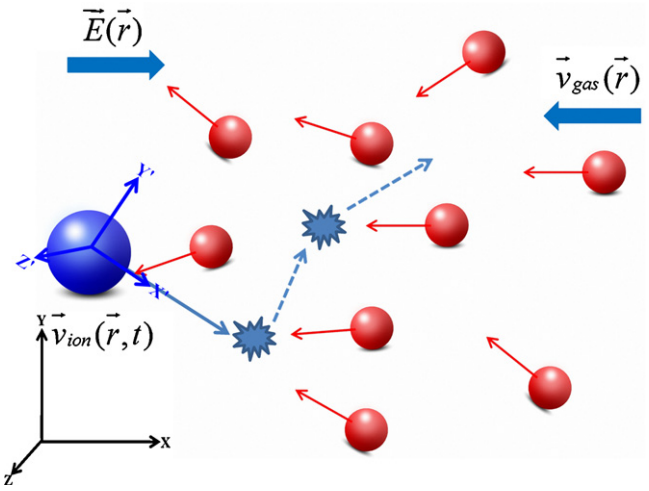

Fig. 2. The process of the ions (blue sphere) moving through the gas flow (red sphere) under the influence of an electric field. A local collision probability is computed at each time based on current ion velocity, ion-gas scattering cross section, local gas flow speed pressure and gas temperature. (For interpretation of the references to color in this figure legend, the reader is referred to the web version of this article.)

reaction region passed through the pulse opened ion shutter and entered the drift region, where they were distinguished according to their drift velocities. Then, the ion current was enlarged by an amplifier of 10^9 V/A factor. Finally, the signal was stored by an oscilloscope (Tektronix TDS2024B, 200 MHz).

3. Results and discussion

3.1. Model and mesh

Before the CFD simulation, a physical model was constructed first based on the IMS geometry. The geometry of the IMS which was used in the simulation according to the experiment instrument is shown in Fig. 4(A).

And then a calculation region called "control volume" should be built, which is the defined volume where the gas flows through shown in Fig. 4(B). In order to reduce the computational time, the physical model was simplified: a 2-dimension control volume was used instead of the 3-dimension volume. For a verification of the model, this simplification was feasible in this process according to the compare with the experiment results. Because of the points in the potential array and gas flow arrays must correspond one-to-one, the dimensions used in the FLUENT are exactly the same as the model used in the SIMION. A finite volume method was used to discretize the control equations on the quadrangle meshes, which were shown in Fig. 4(C). The electrodes model and potential energy view for the IMS used in the experiment and simulation were shown in Fig. 4(D). The ion shutter opened for 200 μs within a 100 ms cycle. The electrical potentials applied to electrodes in normal operation mode were given in Table 1.

Table 1
Operating parameters of the IMS drift tube used in the experiment and simulation.

Electrode	Potential (V)	Electrode	Potential (V)	
Electrode ring 1	360	Electrode ring 9	1800	
Electrode ring 2	540	Ion shutter grid1	2013	
Electrode ring 3	720	Ion shutter grid2	2013/2100	Open/ closed
Electrode ring 4	900	Electrode ring 10	2160	
Electrode ring 5	1080	Electrode ring 11	2340	
Electrode ring 6	1260	Ionized region ring	2650	
Electrode ring 7	1440	Shielded grid	180	
Electrode ring 8	1620	Collector	Grounded	

Table 2
Applied boundary conditions and parameters used in the CFD simulation.

	Boundary type	Value
Inlet	Mass flow inlet	100–1000 ml/min
Outlet	Pressure outlet	101,325 Pa
Wall	No slip/steady temperature	373 K (100 °C)
Drift air temperature	Constant temperature	300 K (27 °C)
Drift air density	Constant	1.25×10^{-3} g/cm^3
Specific heat	Constant	1.00643×107 J/g k
Viscosity	Constant	1.794×10^{-4} P

3.2. Fluid dynamic simulations

Turbulent fluid flow in the IMS was calculated by the CFD package FLUENT, using a finite volume method for the time-averaged Navier–Stokes equations closed by the standard $k-\varepsilon$ turbulence model. The boundary conditions used in the simulation were summarized in Table 2.

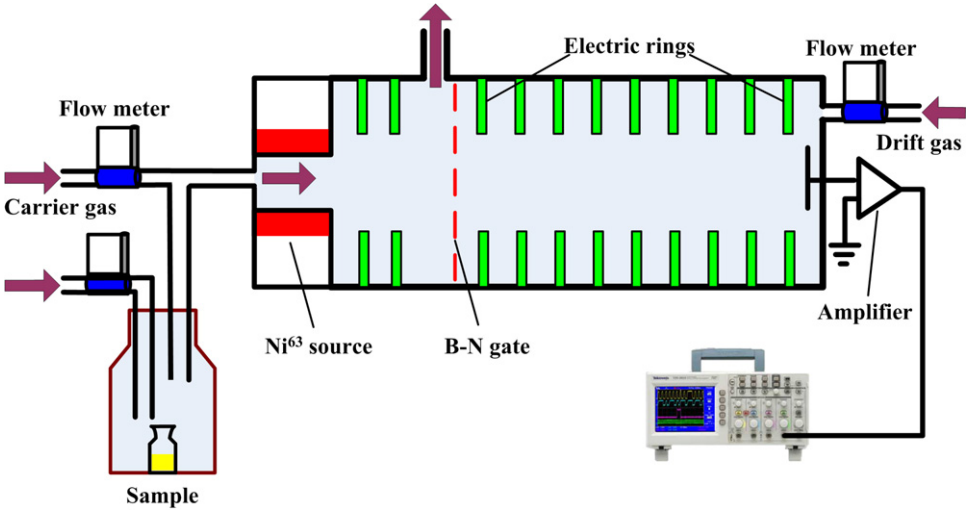

Fig. 3. Schematic diagram of ion mobility spectrometer used for the experiment.

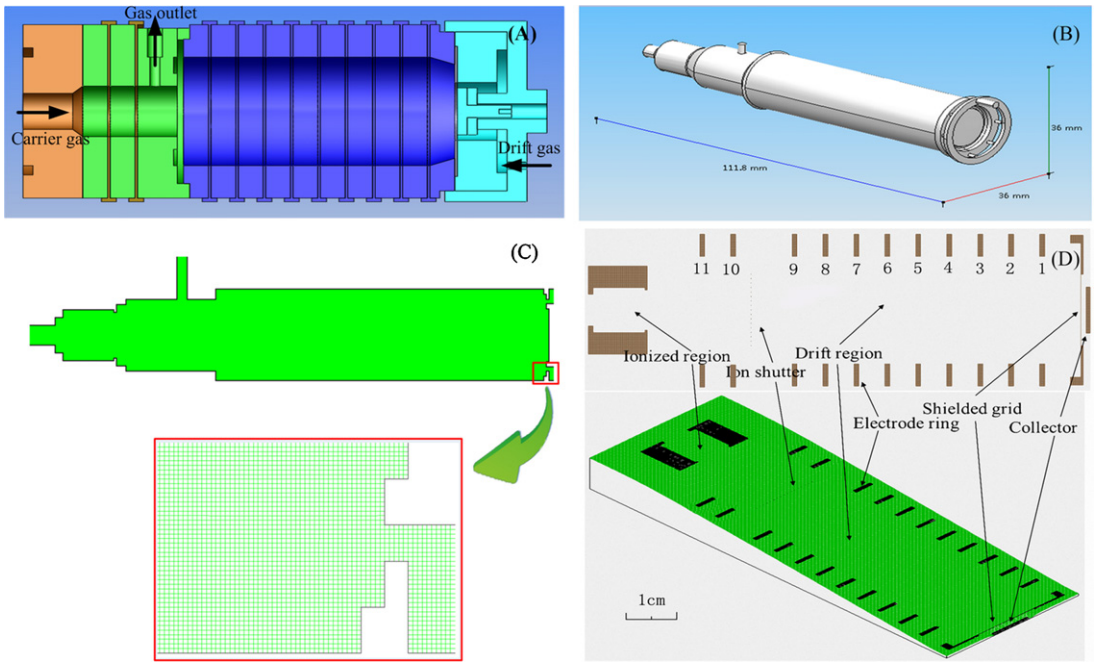

Fig. 4. (A) Geometry of the IMS, (B) the calculation region of the fluid, (C) 2D physical model and quadrangle meshes of the IMS and (D) Electric model and potential energy view for the IMS used in the simulation.

The results shown in Fig. 5 were the distribution of velocity (A), temperature (B) and pressure (C), respectively. In this simulation, the temperature of the IMS wall was 373 K, and the gas flow temperature was the same as the room temperature (300 K). The carrier gas flow rate was 100 ml/min, and the drift gas flow rate was 600 ml/min. It can be seen from Fig. 5(A) that the gas flow was almost steady in the drift region. There was only a little turbulence at the outlet of the tube. The temperature inside the drift tube was demonstrated in Fig. 5(B). A high temperature on the wall could avoid the drift tube contaminated by the sample ions. And we can see clearly that the temperature inside the tube was mainly determined by the drift gas flow temperature. The pressure distribution relative to 1 atm was shown in Fig. 5(C). The pressure was almost constant in the drift tube, but there was a pressure drop at the outlet of the tube. A stable pressure was very helpful for maintaining the ion cluster stable, that was a very important factor for the IMS resolution and signal intensity. The results all above could supply helpful information for the construction improvement of the IMS.

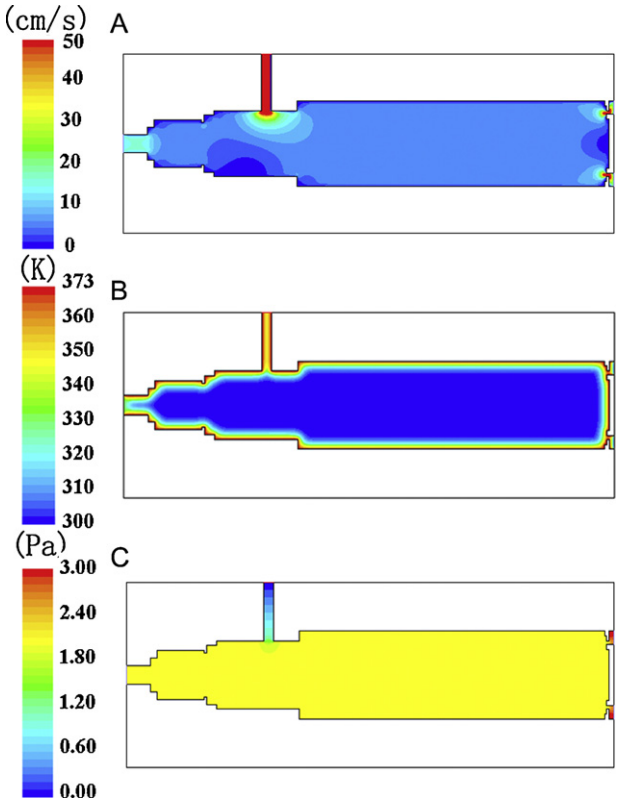

Fig. 5. The field distribution of velocity (A), temperature (B) and pressure (relative to 1 atm) (C) in the IMS tube. The carrier flow rate is 100 ml/min, and drift gas flow rate is 600 ml/min. The gas temperature is 300 K, and the temperature of the wall is 373 K.

The contour of velocity field distribution with the drift gas from 200 ml/min to 1000 ml/min was shown in Fig. 6. Some turbulence could be observed closed to the detector plate when the gas flow increased bigger than 600 ml/min. With the increase of the gas flow, this turbulence gets more evident. This effect can be expected that have some influence on the resolution of the IMS. Besides that the flow in the IMS drift region distributes well, there was no evident turbulence in the drift region.

The results shown in Fig. 7(A) is the velocity at the axis of the IMS for different drift gas flow rate from 200 ml/min to 1000 ml/min. It can be seen clearly that the magnitude of the velocity get larger with the increase of the drift gas flow. And the velocity is nearly constant in the drift region. Fig. 7(B) shows clearly that, with the increased flow rate from the drift gas inlet, the negative $\times$ velocity increased. In the ionization region of the IMS, the gas flow goes though the positive x-axis, while in the drift region it flows though the negative x-axis. The increased drift gas flow slows down the ions by more collisions with the gas molecules, because the gas molecules move faster. The ion motion can be seen more clearly in the ion trajectories simulations of the next step.

3.3. Ion trajectory simulations

The trajectories for 500 ions of $(H_2O)_3H^+$ in the IMS for different drift gas flow from 200 ml/min to 1000 ml/min were shown in Fig. 8. Gauss distribution group ions birthed at random space

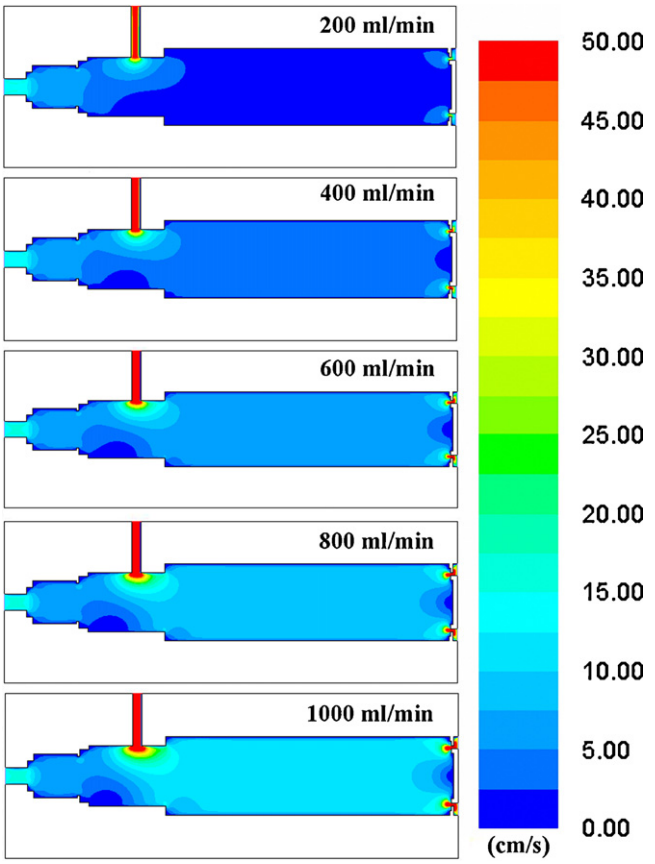

Fig. 6. Distribution of flow velocity inside the IMS with drift gas flow from 200 ml/min to 1000 ml/min.

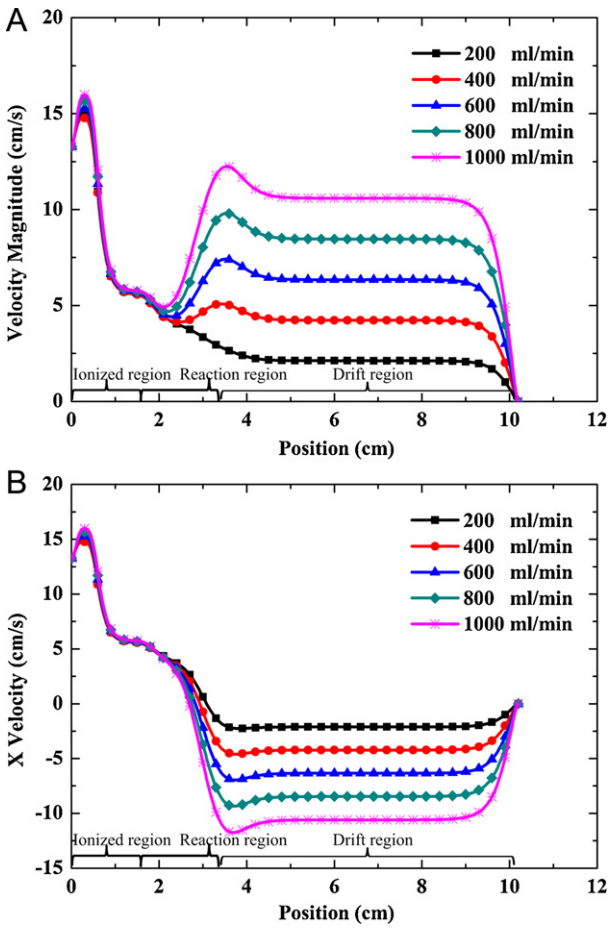

Fig. 7. Velocity magnitude (A) and X velocity (B) at the axis for different drift gas flow.

and time to simulate the process of ionization by a Ni^{63} ionization source. The generated ions moved thought the reaction region by the combined effect of the electric field force and the carrier gas flow. We can see three phenomena: first, there was a very apparent focusing effect at the exit of the ionization region. Second, the ions got some dispersion and make a deviation when they arrived at the ion shutter, which is caused by the gas flow at the IMS outlet. And last, the ions were focused again because of the electric field effect in the drift region. Some of the ions annihilated on the ion shutter grid. That was a very

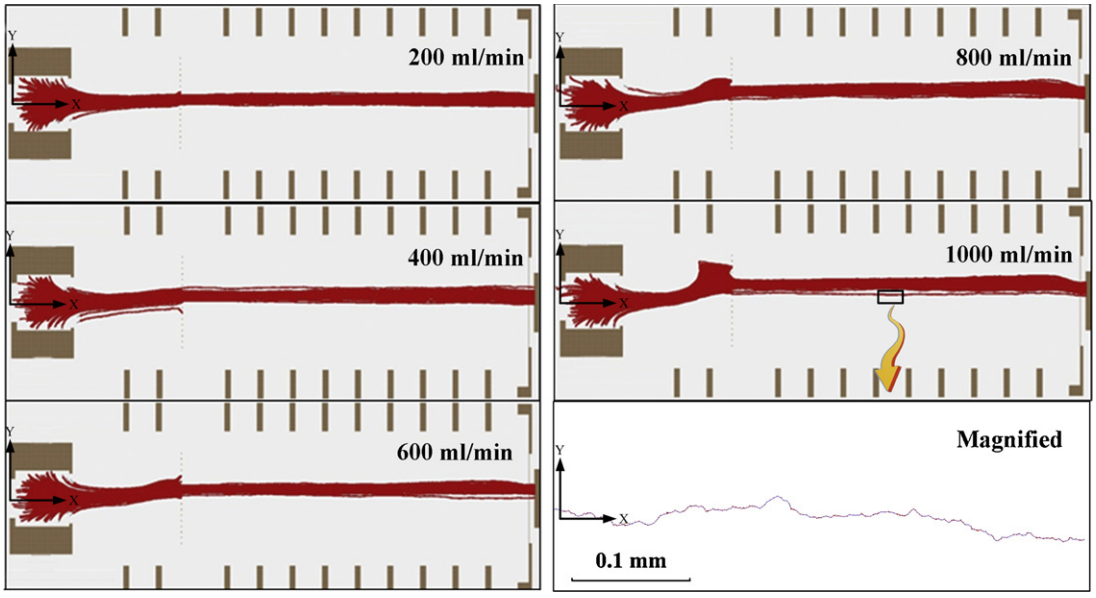

Fig. 8. 500 trajectories of $(H_2O)_3H^+$ ions in the IMS for different drift gas flow from 200 ml/min to 1000 ml/min.

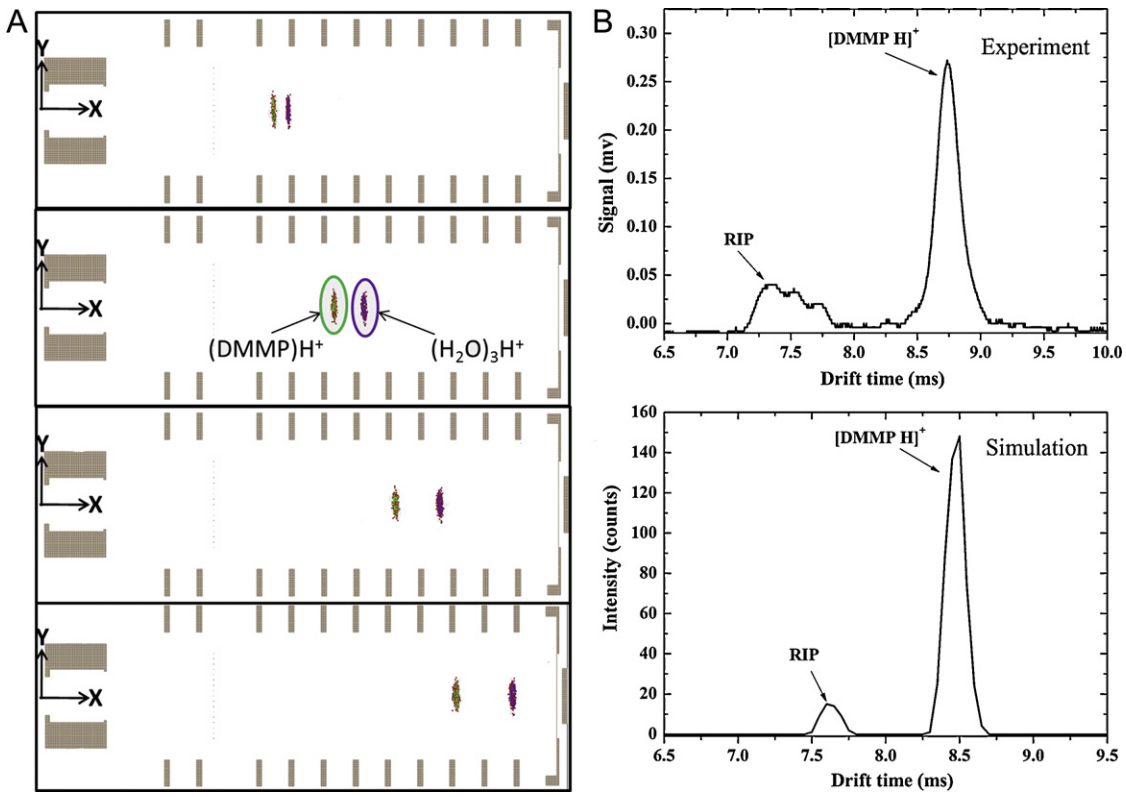

Fig. 9. (A) The distribution of $(DMMP)H^+$ and $(H_2O)_3H^+$ ions at different observation times of 1 ms, 3 ms, 5 ms and 7 ms; (B) experimental (upper) and simulated (below) spectrum of RIP and (DMMP)H+ with 700 ml/min air as the drift gas.

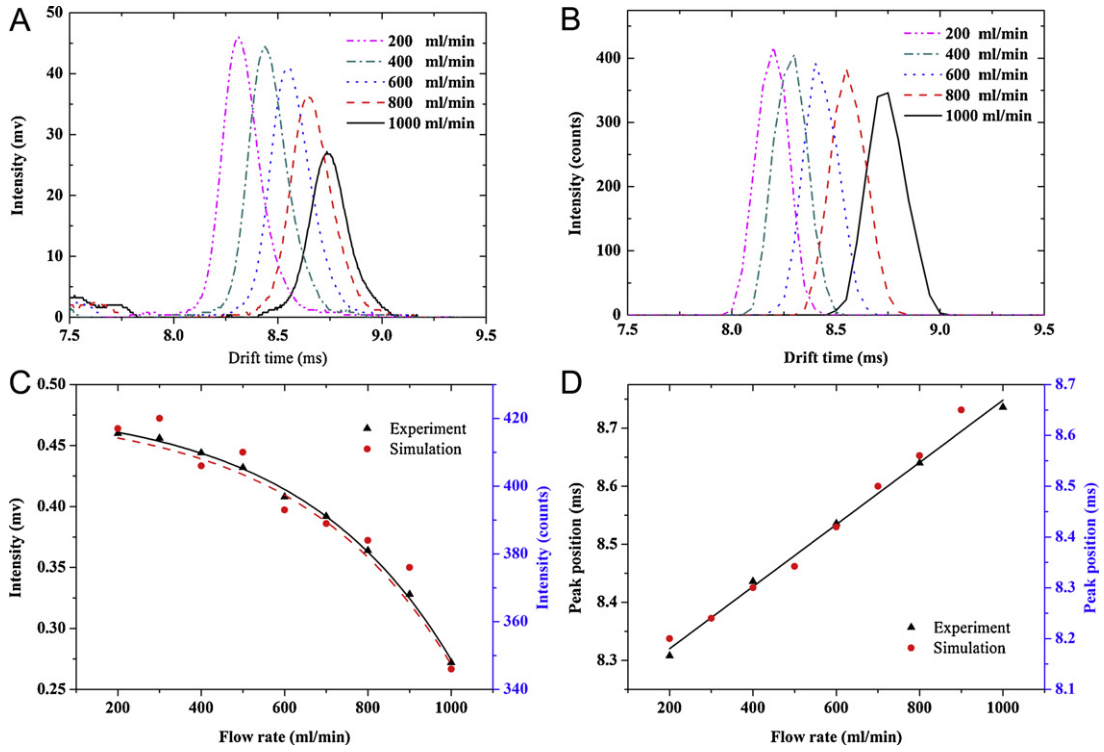

Fig. 10. Experimental (A) and simulated (B) ion mobility spectra of $(DMMP)H^+$; comparison of experimental vs. simulated peak intensity(C) and peak position (D) with different drift gas from 200 ml/min to 1000 ml/min.

important reason for the signal intensity decline. And with a magnification on the trajectory, we can see that the ion moved with random walk. That was caused by the collisions with the buffer gas molecules. So the ions diffuse in the radial direction, which was another reason for the decline of the efficiency. The simulation results can express the ion trajectories and diffusion effect intuitively, which can be a very useful theory expression for the construction and dimension improvement in the future.

3.4. Ion mobility spectrum simulations

To validate the spectrum simulation results, dimethyl methylphosphonate (DMMP) (99.00% Shanghai Adamas-Beta Co., Ltd.) was used as the test compound for flow rate experiments in the positive mode IMS.

In this simulation, the RIP ions were assumed to be $(H_2O)_3H^+$. The effect mass of $(DMMP)H^+$ and $(H_2O)_3H^+$ was set as 125.08 amu and 55 amu [62,63], respectively. The structure effect of the molecular was not considered in the simulation. The mass of background gas particle was set as 28.9 amu. The polarizability of the carrier-gas molecule for the dry air was approximated as 1.73 $Å^3$ [64]. The distribution of $(DMMP)H^+$ and $(H_2O)_3H^+$ ions at different observation times was show in Fig. 9(A). The $(DMMP)H^+$ had more effect mass and collisions cross section than the $(H_2O)_3H^+$ ions. Therefore the collision frequency was higher for the $(DMMP)H^+$, which caused a macro low mobility and thus a long drift time. The separation process of the two kinds of ions in the drift tube was shown in Fig. 9(A). The calculated and experimental ion mobility spectra of RIP and $(DMMP)H^+$ are shown in Fig. 9(B), respectively. The trend of the simulated and experimental results agrees very well. The three small peaks around RIP peak in the experimental spectrum were due to the impurity of the IMS system.

The experimental and simulated spectra of the IMS with different flow rate of drift gas from 200 ml/min to 1000 ml/min were shown in Fig. 10(A) and (B), respectively. We can see clearly that the peak positions move to longer time when the drift gas flow increases. The increasing of drift gas flow caused higher collision frequency, so the velocity of the ions decreased more quickly, which induces a longer drift time of the ions. On the other hand, the maximum of the peak height decrease with the rising of drift gas flow. It is ascribed that with the drift gas flow increasing, the diffusion of the ions increased due to the flight time of the ions increases. The calculated and experimental peak position and intensity under different drift gas flow rate were shown in Fig. 10(C) and (D), respectively. With the drift gas flow increased, the intensity of the peak decreased, while the position of the peak shifted to right. A smaller drift gas flow is helpful for the sensitivity, but a much small drift gas flow will make the drift tube contaminated easier. So selecting a proper drift gas is very important for the IMS sensitivity. The simulated drift times predicted by the model were within 6% deviation with the experiment, the trend of the simulated and experimental results coincided well.

4. Conclusions

A CMC ion trajectory simulation model has been developed based on the ion optics simulation program SIMION 8.0, which considers both the gas flow effect and collision of the ions with the gas molecules. A drift tube ion mobility spectrometer was built and simulated to verify this model. The good agreements between simulated and experimental peak positions and peak heights under different flow rates of drift gas demonstrate that the CMC model has predictive power for modeling ion motion at ambient pressure, and this model can serve as visual aids for intuitively understanding the factors that determine ion transport at ambient pressure.

Acknowledgements

This work was supported by the National Natural Science Foundation of China (Nos. 20573111 and 40637036), the National High-Tech Research and Development Plan (No. 2007AA061503), and the Major Subject of The Chinese Academy of Sciences (No. Y2005005).

References

[1] G.A. Eiceman (Ed.), Ion Mobility Spectrometry, 2nd ed., CRC Press, New Mexico, 2005.
[2] G.A. Eiceman, E.G. Nazarov, J.E. Rodriguez, J.A. Stone, Analysis of a drift tube at ambient pressure: models and precise measurements in ion mobility spectrometry, Rev. Sci. Instrum. 72 (2001) 3610–3621.
[3] I.A. Buryakov, E.V. Krylov, A.L. Makas, E.G. Nazarov, V.V. Pervukhin, U.K. Rasulev, Separation of ions according to mobility in a strong ac electric field, Sov. Tech. Phys. Lett. 16 (1991) 446.
[4] I.A. Buryakov, E.V. Krylov, E.G. Nazarov, A new method of separation of multi-atomic ions by mobility at atmospheric pressure using a high-frequency amplitude-asymmetric strong electric field, Int. J. Mass Spectrom. Ion Process. 128 (1993) 143–148.
[5] R. Guevremont, High-field asymmetric waveform ion mobility spectrometry: a new tool for mass spectrometry, J. Chromatogr. 1058 (2004) 3–19.
[6] R. Guevremont, High-field asymmetric waveform ion mobility spectrometry (FAIMS), Can. J. Anal. Sci. Spectrosc. 49 (2004) 105–113.
[7] A.V. Tolmachev, T. Kim, H.R. Udseth, R.D. Smith, T.H. Bailey, J.H. Futrell, Simulation-based optimization of the electrodynamic ion funnel for high sensitivity electrospray ionization mass spectrometry, Int. J. Mass Spectrom. 203 (2000) 31–47.
[8] R.T. Kelly, A.V. Tolmachev, J.S. Page, K.Q. Tang, R.D. Smith, The ion funnel: theory, implementations, and applications, Mass Spectrom. Rev. 29 (2010) 294–312.
[9] M.W. Forbes, M. Sharifi, T. Croley, Z. Lausevic, R.E. March, Simulation of ion trajectories in a quadrupole ion trap: a comparison of three simulation programs, J. Mass Spectrom. 34 (1999) 1219–1239.
[10] S.D. Harvey, R.G. Ewing, M.J. Waltman, Selective sampling with direct ion mobility spectrometric detection for explosives analysis, Int. J. Ion Mob. Spec. 12 (2009) 115–121.
[11] D. Morgos, I. Geroy, R.G. Sevier, M.M. Gribb, K.P. Ryan, H.H. Hill, An ion mobility spectrometer sensor system for subsurface use, Int. J. Ion Mob. Spec. 13 (2009) 1–7.
[12] S.L. Coy, E.V. Krylov, B.B. Schneider, T.R. Covey, D.J. Brenner, J.B. Tyburski, A.D. Patterson, K.W. Krausz, A.J. Fornace, E.G. Nazarova, Detection of radiation-exposure biomarkers by differential mobility prefiltered mass spectrometry (DMS-MS), Int. J. Mass Spectrom. 291 (2010) 108–117.
[13] H. Borsdorf, E.G. Nazarov, R.A. Miller, Time-of-flight ion mobility spectrometry and differential mobility spectrometry: a comparative study of their efficiency in the analysis of halogenated compounds, Talanta 71 (2007) 1804–1812.
[14] E. Nazarov, R. Miller, G. Eiceman, E. Krylov, B. Tadjikov, Effect of the electric field strength, drift gas flow rate, and temperature on RF IMS response, Int. J. Ion Mob. Spec. 4 (2001) 43–46.
[15] R. Fernandez-Maestre, C. Wu, H.H. Hill, Using a buffer gas modifier to change separation selectivity in ion mobility spectrometry, Int. J. Mass Spectrom. 298 (2010) 2–9.
[16] R. Fernandez-Maestre, C.S. Harden, R.G. Ewing, C.L. Crawford, H.H. Hill, Chemical standards in ion mobility spectrometry, Analyst 135 (2010) 1433–1442.
[17] M. Westhoff, P. Litterst, L. Freitag, W. Urfer, S. Bader, J.I. Baumbach, Ion mobility spectrometry for the detection of volatile organic compounds in exhaled breath of patients with lung cancer: results of a pilot study, Thorax 64 (2009) 744–748.
[18] S. Myung, J.M. Wiseman, S.J. Valentine, Z. Takats, R.G. Cooks, D.E. Clemmer, Coupling desorption electrospray ionization with ion mobility/mass spectrometry for analysis of protein structure: evidence for desorption of folded and denatured states, J. Phys. Chem. B 110 (2006) 5045–5051.
[19] P. Dwivedi, C. Wu, L.M. Matz, B.H. Clowers, W.F. Siems, H.H. Hill, Gas-phase chiral separations by ion mobility spectrometry, Anal. Chem. 78 (2006) 8200–8206.
[20] C. Eckers, A.M.F. Laures, K. Giles, H. Major, S. Pringle, Evaluating the utility of ion mobility separation in combination with high-pressure liquid chromatography/mass spectrometry to facilitate detection of trace impurities in formulated drug products, Rapid Commun. Mass Spectrom. 21 (2007) 1255–1263.
[21] P. Dwivedi, A.J. Schultz, H.H. Hill, Metabolic profiling of human blood by high-resolution ion mobility mass spectrometry (IM-MS), Int. J. Mass Spectrom. 298 (2010) 78–90.
[22] A.B. Kanu, G. Hampikian, S.D. Brandt, H.H. Hill, Ribonucleotide and ribonucleoside determination by ambient pressure ion mobility spectrometry, Anal. Chim. Acta 658 (2010) 91–97.
[23] S.K. Guharay, P. Dwivedi, H.H. Hill, Ion mobility spectrometry: ion source development and applications in physical and biological sciences, IEEE Trans. Plasma Sci. 36 (2008) 1458–1470.
[24] L.M. Matz, P.S. Tornatore, H.H. Hill, Evaluation of suspected interferents for TNT detection by ion mobility spectrometry, Talanta 54 (2001) 171–179.
[25] G.R. Asbury, J. Klasmeier, H.H. Hill, Analysis of explosives using electrospray ionization/ion mobility spectrometry (ESI/IMS), Talanta 50 (2000) 1291–1298.

[26] Z. Ouyang, R.G. Cooks, Miniature mass spectrometers, Annu. Rev. Anal. Chem. 2 (2009) 187–214.
[27] R.G. Cooks, Z. Ouyang, Z. Takats, J.M. Wiseman, Ambient mass spectrometry, Science 311 (2006) 1566–1570.
[28] C. Dong, W. Wang, H. Li, Atmospheric pressure air direct current glow discharge ionization source for ion mobility spectrometry, Anal. Chem. 80 (2008) 3925–3930.
[29] C. Chen, C. Dong, Y. Du, S. Cheng, F. Han, L. Li, W. Wang, K. Hou, H. Li, Bipolar ionization source for ion mobility spectrometry based on vacuum ultraviolet radiation induced photoemission and photoionization, Anal. Chem. 82 (2010) 4151–4157.
[30] R.C. Blase, J.A. Silveira, K.J. Gillig, C.M. Gamage, D.H. Russell, Increased ion transmission in IMS: a high resolution, periodic-focusing DC ion guide ion mobility spectrometer, Int. J. Mass Spectrom. 301 (2011) 166–173.
[31] J.A. Silveira, C.M. Gamage, R.C. Blase, D.H. Russell, Gas-phase ion dynamics in a periodic-focusing DC ion guide, Int. J. Mass Spectrom. 296 (2010) 36–42.
[32] C.M. Gamage, J.A. Silveira, R.C. Blase, D.H. Russell, Gas-phase ion dynamics in a periodic-focusing DC ion guide (part II): discrete transport modes, Int. J. Mass Spectrom. 303 (2011) 154–163.
[33] A.V. Tolmachev, H.R. Udseth, R.D. Smith, Modeling the ion density distribution in collisional cooling RF multipole ion guides, Int. J. Mass Spectrom. 222 (2003) 155–174.
[34] C.L. Hendrickson, S.C. Beu, G.T. Blakney, A.G. Marshall, SIMION modeling of ion image charge detection in Fourier transform ion cyclotron resonance mass spectrometry, Int. J. Mass Spectrom. 283 (2009) 100–104.
[35] I.M. Taban, L.A. McDonnell, A. Römpp, I. Cerjak, R.M.A. Heeren, SIMION analysis of a high performance linear accumulation octopole with enhanced ejection capabilities, Int. J. Mass Spectrom. 244 (2005) 135–143.
[36] K.M. Roscioli, E. Davis, W.F. Siems, A. Mariano, W. Su, S.K. Guharay, H.H. Hill, Modular ion mobility spectrometer for explosives detection using corona ionization, Anal. Chem. (2011).
[37] W. Vautz, S. Sielemann, J.I. Baumbach, 3D gas flow simulation as a tool for the characterisation and optimisation of ion mobility spectrometers, Int. J. Ion Mob. Spec. 7 (2004) 19.
[38] H.J. Schmid, L. Vogel, On the modelling of the particle dynamics in electrohydrodynamic flow-fields: I. Comparison of Eulerian and Lagrangian modelling approach, Powder Technol. 135 (2003) 118–135.
[39] H.A. Bui, R. Graham Cooks, Windows version of the ion trap simulation program ITSIM: a powerful heuristic and predictive tool in ion trap mass spectrometry, J. Mass Spectrom. 33 (1998) 297–304.
[40] R.G. Cooks, Report: Ion Motion and Ion Excitation in the Quadrupole Ion Trap Mass Spectrometer:Simulation and Experiment, Purdue University, West Lafayette, IN, 2005.
[41] G. Wu, R.G. Cooks, Z. Ouyang, M. Yu, W.J. Chappell, W.R. Plass, Ion trajectory simulation for electrode configurations with arbitrary geometries, J. Am. Soc. Mass Spectrom. 17 (2006) 1216–1228.
[42] A. Hieke, S.R.Weinberger, An Advanced Laser Desorption Ionization Ion Source with Controlled Superposition of Electric and Pneumatic Fields. 53rd ASMS Conference on Mass Spectrometry and Allied Topics, June 5–9 (2005), San Antonio, TX.
[43] A. Hieke, 3D electro-pneumatic Monte-Carlo simulations of ion trajectories and temperatures during RF quadrupole injection in the presence of gas flow fields, in: 52nd ASMS Conference on Mass Spectrometry and Allied Topics, Nashville, TN, 2004.
[44] E.G. Nazarov, R.A. Miller, S.L. Coy, E. Krylov, S.I. Kryuchkov, Software simulation of ion motion in DC and AC electric fields including fluid-flow effects, Int. J. Ion Mob. Spec. 1 (2006) 40–44.
[45] D.A. Dahl, SIMION Version 8.0 User Manual, 4th ed., Idaho National Laborotary, 2008.
[46] J. Xu, W.B. Whitten, Monte Carlo simulation of ion transport in ion mobility spectrometry, Int. J. Ion Mob. Spec. 11 (2008) 13–17.
[47] J. Xu, Y. Liu, Monte Carlo simulation of ion transport in non-linear ion mobility spectrometry, Int. J. Ion Mob. Spec. 12 (2009) 149–156.
[48] R. Cumeras, I. Gràcia, E. Figueras, L. Fonseca, J. Santander, M. Salleras, C. Calaza, N. Sabaté, C. Cané, Modelling a P-FAIMS with multiphysics FEM, J. Math. Chem. (2010) 1–15.
[49] D.A. Dahl, T.R. McJunkin, J.R. Scott, Comparison of ion trajectories in vacuum and viscous environments using SIMION: insights for instrument design, Int. J. Mass Spectrom. 266 (2007) 156–165.
[50] A.D. Appelhans, D.A. Dahl, SIMION ion optics simulations at atmospheric pressure, Int. J. Mass Spectrom. 244 (2005) 1–14.
[51] H. Lai, T.R. McJunkin, C.J. Miller, J.R. Scott, J.R. Almirall, The predictive power of SIMION/SDS simulation software for modeling ion mobility spectrometry instruments, Int. J. Mass Spectrom. 276 (2008) 1–8.
[52] S. Prasad, K.Q. Tang, D. Manura, D. Papanastasiou, R.D. Smith, Simulation of ion motion in FAIMS through combined use of SIMION and modified SDS, Anal. Chem. 81 (2009) 8749–8757.
[53] A.A. Shvartsburg, K.Q. Tang, R.D. Smith, FAIMS operation for realistic gas flow profile and asymmetric waveforms including electronic noise and ripple, J. Am. Soc. Mass Spectrom. 16 (2005) 1447–1455.
[54] K.J. Gillig, B.T. Ruotolo, E.G. Stone, D.H. Russell, An electrostatic focusing ion guide for ion mobility-mass spectrometry, Int. J. Mass Spectrom. 239 (2004) 43–49.
[55] L. Ding, M. Sudakov, S. Kumashiro, A simulation study of the digital ion trap mass spectrometer, Int. J. Mass Spectrom. 221 (2002) 117–138.
[56] B.E. Launder, D.B. Spalding, Lectures in mathematical models of turbulence, Academic Press, New York, 1972.
[57] FLUENT, FLUENT 6.3 User's Guide, Fluent Inc., Lebanon, USA, 2006.
[58] S.V. Patankar, Numerical Heat Transfer and Fluid Flow, Hemisphere Pub, 1980.
[59] D.A. Dahl, SIMION for the personal computer in reflection, Int. J. Mass Spectrom. 200 (2000) 3–26.
[60] L.W. Beegle, I. Kanik, L. Matz, H.H. Hill, Effects of drift-gas polarizability on glycine peptides in ion mobility spectrometry, Int. J. Mass Spectrom. 216 (2002) 257–268.
[61] C. Dong, L. Wang, W. Wang, K. Hou, H. Li, Dopant-enhanced atmospheric pressure glow discharge ionization source for ion mobility spectrometry, Rev. Sci. Instrum. 79 (2008) 104101.
[62] G.A. Eiceman, E.G. Nazarov, J.A. Stone, Chemical standards in ion mobility spectrometry, Anal. Chim. Acta 493 (2003) 185–194.
[63] G. Kaur-Atwal, G. O'Connor, A. Aksenov, V. Bocos-Bintintan, C. Paul Thomas, C. Creaser, Chemical standards for ion mobility spectrometry: a review, Int. J. Ion Mob. Spec. 12 (2009) 1–14.
[64] L.W. Beegle, I. Kanik, L. Matz, H.H. Hill, Electrospray ionization high-resolution ion mobility spectrometry for the detection of organic compounds, 1. Amino acids, Anal. Chem. 73 (2001) 3028–3034.